

Active degradation of MarA controls coordination of its downstream targets

Nicholas A Rossi, Thierry Mora, Aleksandra M Walczak, Mary J Dunlop

▶ **To cite this version:**

Nicholas A Rossi, Thierry Mora, Aleksandra M Walczak, Mary J Dunlop. Active degradation of MarA controls coordination of its downstream targets. PLoS Computational Biology, 2018, 14 (12), pp.e1006634. 10.1371/journal.pcbi.1006634 . hal-01983208

HAL Id: hal-01983208

https://hal.sorbonne-universite.fr/hal-01983208

Submitted on 16 Jan 2019

HAL is a multi-disciplinary open access archive for the deposit and dissemination of scientific research documents, whether they are published or not. The documents may come from teaching and research institutions in France or abroad, or from public or private research centers.

L'archive ouverte pluridisciplinaire **HAL**, est destinée au dépôt et à la diffusion de documents scientifiques de niveau recherche, publiés ou non, émanant des établissements d'enseignement et de recherche français ou étrangers, des laboratoires publics ou privés.

PLOS COMPUTATIONAL BIOLOGY

RESEARCH ARTICLE

Active degradation of MarA controls coordination of its downstream targets

Nicholas A. Rossi[1,2], **Thierry Mora**[3☯], **Aleksandra M. Walczak**[4☯], **Mary J. Dunlop**[1,2,5*]

1 Molecular Biology, Cell Biology & Biochemistry Program, Boston University, Boston, Massachusetts, United States of America, **2** Biological Design Center, Boston University, Boston, Massachusetts, United States of America, **3** Laboratoire de Physique Statistique, CNRS, Sorbonne Université, Université Paris-Diderot, and École Normale Supérieure (PSL), Paris, France, **4** Laboratoire de Physique Théorique, CNRS, Sorbonne Université, and École Normale Supérieure (PSL), Paris, France, **5** Department of Biomedical Engineering, Boston University, Boston, Massachusetts, United States of America

☯ These authors contributed equally to this work.
* mjdunlop@bu.edu

Check for updates

OPEN ACCESS

Citation: Rossi NA, Mora T, Walczak AM, Dunlop MJ (2018) Active degradation of MarA controls coordination of its downstream targets. PLoS Comput Biol 14(12): e1006634. https://doi.org/10.1371/journal.pcbi.1006634

Editor: Gabor Balazsi, Stony Brook University, UNITED STATES

Received: June 6, 2018

Accepted: November 8, 2018

Published: December 27, 2018

Copyright: © 2018 Rossi et al. This is an open access article distributed under the terms of the Creative Commons Attribution License, which permits unrestricted use, distribution, and reproduction in any medium, provided the original author and source are credited.

Data Availability Statement: All relevant data are within the paper and its Supporting Information files. Raw data sets and code are available at: https://github.com/NicholasARossi/MarA-Halflife-2018

Funding: This research was supported by the National Science Foundation (grant No. 1347635 to MJD), the National Institutes of Health (grant No. 1R01AI102922 to MJD), and a Chateaubriand Fellowship (NAR). The funders had no role in study design, data collection and analysis, decision to publish, or preparation of the manuscript.

Abstract

Several key transcription factors have unusually short half-lives compared to other cellular proteins. Here, we explore the utility of active degradation in shaping how the multiple antibiotic resistance activator MarA coordinates its downstream targets. MarA controls a variety of stress response genes in *Escherichia coli*. We modify its half-life either by knocking down the protease that targets it via CRISPRi or by engineering MarA to protect it from degradation. Our experimental and analytical results indicate that active degradation can impact both the rate of coordination and the maximum coordination that downstream genes can achieve. In the context of multi-gene regulation, trade-offs between these properties show that perfect information fidelity and instantaneous coordination cannot coexist.

Author summary

Very few proteins are actively degraded in bacteria, and those that are tend to be regulatory molecules. One example is MarA, which is a master regulator of stress response in *E. coli*. To study the role of active degradation, we decreased the degradation of MarA two ways: either by knocking down the protease that degrades it, or by modifying MarA to make it resistant to degradation. We measured how changes to the half-life of MarA change the way MarA's downstream genes are coordinated over time. Combining these results with a theoretical model shows that active degradation in MarA represents a trade-off favoring an increased rate of coordination over high maximum coordination. By combining experimental results with a theoretical framework, this research provides new insights into the advantages and disadvantage of actively degrading MarA.

Introduction

Active degradation is a rare feature in bacteria, affecting only 2–7% of total cellular proteins in *Escherichia coli* [1,2]. Active degradation is accomplished by ATP-dependent proteases such as ClpXP, HflB, and Lon [3]. These proteases play a role in protein quality control by degrading

Competing interests: The authors have declared that no competing interests exist.

misfolded proteins [4–6], but they can also degrade functional proteins. Active degradation of functional proteins can serve as a type of post-translational regulation to modify protein concentration [7]. This can be important in time-sensitive processes when removal through dilution is insufficient. Metabolic processes that incorporate active degradation include DNA damage repair, gene expression during stationary-phase, cell division, filamentation, and accelerated removal of certain regulatory proteins [8,9]. Although active degradation can play a regulatory role, this comes with an energy cost due to the ATP necessary to activate the proteases, and a metabolic investment required to replace degraded proteins [10]. Active degradation occurs in many other microorganisms as well, such as with the ComK regulator of sporulation in *Bacillus subtilis* [11] and in many regulatory proteins in humans including the p53 tumor suppressor [12,13] and IκBα, which dictates NF-κB activity and cellular stress response [14,15]. The refractory period of NF-κB pulses is determined by this degradation rate, which dictates the limit of information transmission in the system [16]. In eukaryotes, the percentage of proteins that are primarily removed through active degradation ranges from ~15% in yeast [17] to ~50% in humans [18]. Therefore, despite active degradation's role in regulation across domains of life, it is still comparatively rare in bacteria due to their rapid growth rate, which produces stronger dilution effects. The relative rarity coupled with the cost implicit to active degradation makes the presence of any short half-life protein in bacteria conspicuous. What potential utility could necessitate the use of this rare design feature?

To answer this, we focused on the multi-antibiotic resistance activator (MarA) in *E. coli* as a case study. MarA has a short half-life even by the standards of an actively degraded protein, with an estimated half-life of 1–3 minutes due to Lon protease activity [19,20]. Moreover, MarA regulates over 60 downstream targets involved in a variety of antibiotic resistance roles, from genes encoding efflux pump components like *acrAB* and *tolC* to stress response proteins like *inaA* [21,22]. The majority of the downstream genes encode for stable proteins, therefore MarA has a much shorter half-life than most of its downstream targets [21]. MarA is part of a greater regulon, where three homologous proteins—MarA, Rob, and SoxS—regulate an overlapping suite of downstream genes [23]. However, MarA's clear correlation with phenotypic outcomes make it an ideal target for studying why evolution would select for actively degraded regulatory molecules [24].

Recent studies have revealed that *marA* is expressed stochastically, creating phenotypic diversity within isogenic populations. This noisy expression is linked to transient antibiotic resistance [24]. Thus, stochastic expression of *marA* can impact whether a cell lives or dies under antibiotic exposure. At the population level, there is a distribution of MarA levels where some cells are antibiotic resistant and others are susceptible. This may serve as a bet hedging strategy, where cells with high *marA* expression act as insurance policy to protect against the sudden appearance of antibiotics or other stressors.

In conditions with small numbers of cells, the rate at which diversity in MarA levels is generated is important. Starting with a single cell at a single time point, there is no diversity. As the cell grows and divides, diversity develops within the population. The rate at which this diversity develops depends on the time scale of the stochastic dynamics of the genes being expressed, including their rate of degradation [11,25]. We measure diversity as the distribution of distinct protein concentrations present in a population. The half-life of the protein impacts the rate of diversity generation and the maximum diversity achieved (Fig 1A). For a regulatory protein such as MarA (X), phenotypic diversity can propagate to its downstream targets such as AcrAB and InaA (Y and Z) (Fig 1B). The rate at which diversity appears in downstream genes is impacted by how the upstream regulator changes with time. Active degradation affects the variability in the activator concentration—how quickly the concentration changes in one cell over time, as well as the diversity in concentrations between cells. This produces a

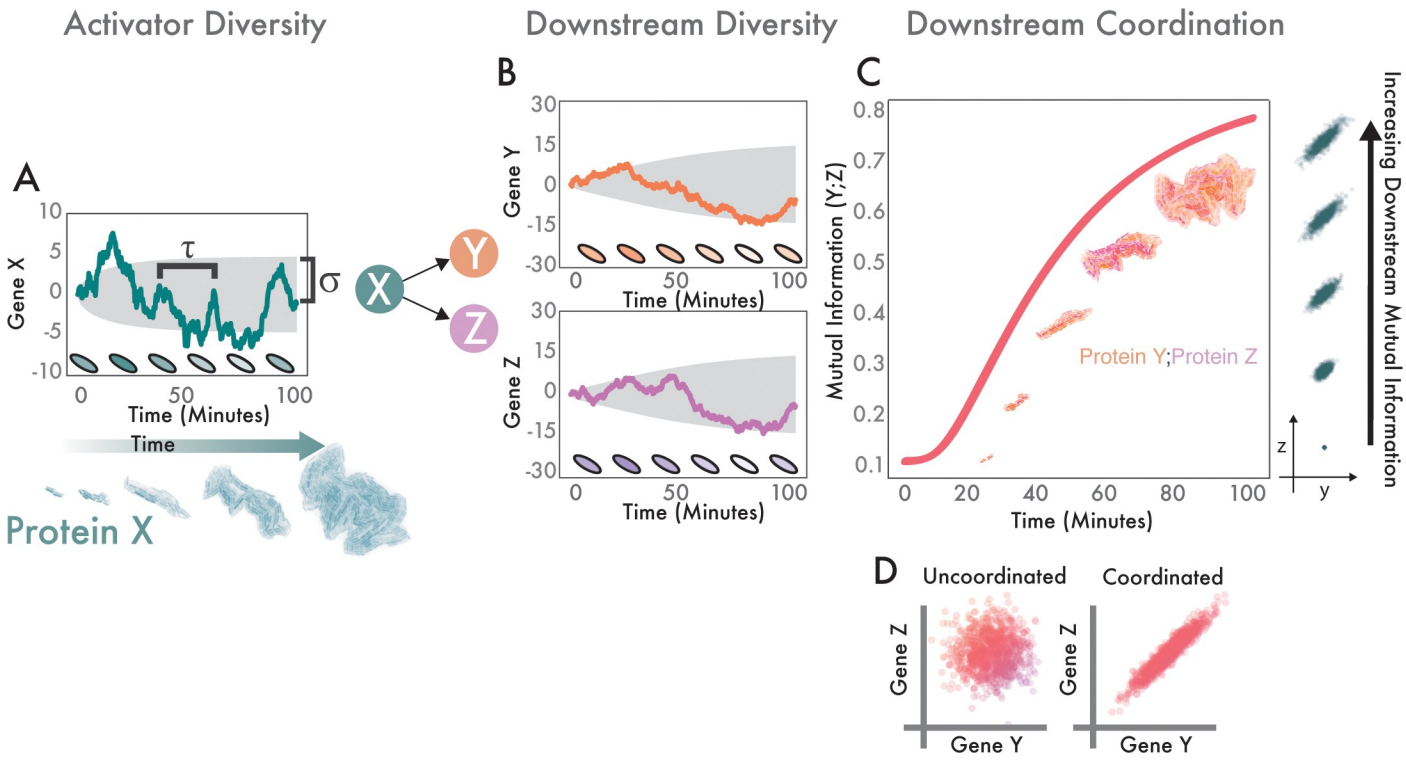


Fig 1. Statistics of stochastic protein expression in individual cells determine coordinated diversity in populations. (A) Variability in the master regulator (X) expands over time. Teal trace corresponds to a simulation of a single stochastic protein trajectory in one cell for a protein half-life of 30 minutes; shaded cells illustrate how we expect this to appear *in vivo*. τ governs how quickly the trace changes in time and scales with the protein half-life. Shaded gray region (σ) shows analytical solutions of how the projected diversity evolves over time (one standard deviation around the mean). Below, experimental data from growing microcolony shows how individual heterogeneity in MarA becomes population-level diversity. **(B)** Activator diversity propagates to downstream genes. This mirrors the architecture of MarA and two of its many downstream targets. Colored traces and gray shaded regions are the same as (A), but for Y and Z instead of X. **(C)** X produces growing coordinated diversity in Y and Z. Pink trace shows how coordinated diversity increases over time. Gray point clouds show how increasing information between two downstream targets appears visually. Experimental data from growing microcolony shows how heterogeneity between individual cells produces population-level variability in InaA and AcrAB. **(D)** Comparison between uncoordinated and coordinated downstream genes. Left scatter plot indicates two genes not governed by a master regulator. They have high variability, but low coordination. Right plot shows equally high variability, but increased coordination due to a common regulator.

https://doi.org/10.1371/journal.pcbi.1006634.g001

spectrum of phenotypes where individual cells exhibit a range from low to high expression for all downstream targets (Fig 1C). This coordinated diversity in expression of genes that share a master regulator is different from the uncoordinated diversity in two uncoupled genes (Fig 1D). We used mutual information to quantify increasing coordination of downstream genes. Mutual information describes how well knowing the concentration of one of these proteins allows us to predict the concentration of the other [26]. It measures their co-expression properties even if the correlation between them is nonlinear, an important feature because transcriptional dose response curves typically saturate, following the shape of a Hill function [27]. S1 Movie shows an animation of how stochastic expression of an activator produces coordinated diversity within downstream targets.

Coordination as a function of a shared master regulator is important for establishing synergistic effects between downstream targets. For instance, MarA activates expression of genes in the AcrAB-TolC efflux pump, the small RNA *micF* which decreases porin expression, and other stress response genes such as *inaA*. Conceptually, expressing multiple genes is like locking both the front door and the back door to a home in order to protect it; locking just one door makes the home only marginally safer and expends energy. Thus, coordinating expression of stress response genes is essential.

Here, we investigate the role of activator half-life in controlling how a stochastic regulator generates coordinated diversity in multiple downstream genes. We do this by controlling the half-life of MarA, either by modulating the concentration of Lon protease or by protecting MarA itself from proteolytic degradation. We then evaluate the impact of MarA's half-life by computing both the maximum amount of coordinated diversity that MarA can achieve as well as the rate at which it achieves it.

Results

We first developed an analytic model of how noise in MarA propagates to downstream genes as a function of its half-life to generate predictions that we could test experimentally. In the model, an upstream regulator (X) activates two downstream proteins (Y and Z). We modeled noise in X using an Ornstein-Uhlenbeck process [27–29]. The simulation and analytical results from this model produce results in terms of units of concentration of X. The model has two free parameters: τ, which is a scaled version of the half-life of the molecule ($\tau = \lambda/\ln(2)$, where λ is the half-life) and σ, which specifies the noise in protein expression (Methods). Using this model, τ changes the dynamics of the process as well as the population distribution that such a process can produce (Fig 2A). The stochastic simulations demonstrate that having a longer half-life causes the protein concentration to change more slowly–negative values indicate a lower concentration than the mean, positive values indicate a higher concentration. Additionally, the longer half-life allows the trajectory of protein concentration to wander farther away from the mean, increasing the standard deviation (Fig 2A). In this case, σ = 1 and the standard deviation scales as $\sqrt{\tau/2}$ [28]. Analytical solutions to these functions show that as the half-life of a molecule increases, it takes longer to reach the maximum variability (Fig 2B). Here, variability is measured as variance because it is a zero mean process (S1 File).

Variability in a regulatory molecule propagates to the downstream genes it controls. To quantify the correlation between the concentrations of two downstream proteins (Y and Z) regulated by X, we measured the mutual information between their concentrations as a function of time. First, we observed an apparent advantage to longer half-life activators, as increasing half-life increases the mutual information between two downstream targets (Fig 2C). Large variability in the activator concentration allows for coordinated diversity in the downstream genes, and a longer half-life molecule produces greater information between the two downstream genes. The decreased mutual information of short half-life activators is due to filtering of high-frequency changes. Downstream genes function as low-pass filters in which signals that change quickly are averaged out [30]. Moreover, because increasing the half-life increases the standard deviation of protein levels, the variability in downstream genes increases as well, allowing for a greater range of coordinated activation. These results show that longer half-life proteins may be better at generating coordinated diversity in downstream targets. However, this conclusion is dependent on allowing the standard deviation to scale freely with the half-life of the regulatory molecule.

To validate these analytic predictions, we designed a genetic system to modify the concentration of Lon protease. Changing the concentration of Lon should change the statistics of MarA and the downstream genes it regulates. We used CRISPRi to knock down Lon expression, allowing us to control the level of MarA. We first transformed *E. coli* with dCas9 and a sgRNA targeting *lon* [31]. Lon protease knockouts have been shown to increase the half-life of MarA to ~30 minutes, therefore increasing the mean concentration MarA in *E. coli*, but this change affects other genes in addition to *marA* [19,32]. In order to avoid off-target pleiotropic effects from eliminating Lon protease such as cell filamentation [33], we designed the sgRNA to increase MarA levels, but to produce no qualitative morphological changes to the cell (S1

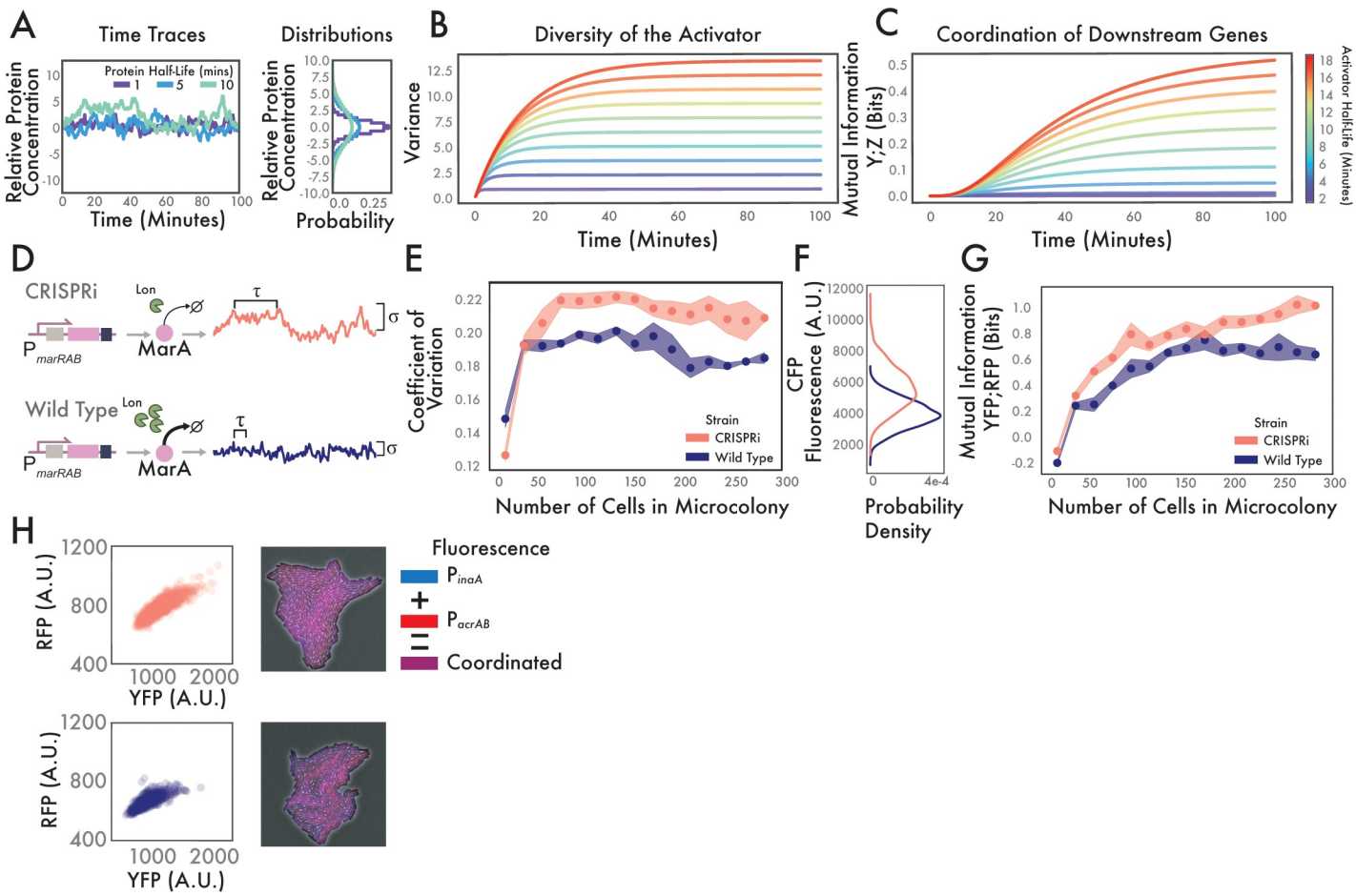


Fig 2. CRISPRi knockdown of Lon protease to increase half-life. (A) Simulation of how the half-life of regulator X affects correlation time and variability. Sample trajectories with varying degradation rates produce different probability distributions (right). Negative and positive values indicate relative changes in concentration compared to the mean. **(B)** Analytical solutions for the variability of a protein as a function of differing half-lives. Individual traces demonstrate increasing variance as a function of time and the half-life. **(C)** Analytical solutions for the coordination of two downstream genes as a function of differing activator half-lifes. Individual traces demonstrate increasing coordination in two downstream genes as a function of time and the half-life of the activator. **(D)** Experimental schematic for CRISPRi knockdown of Lon protease. Upper row shows how time-constant τ and the noise scaling term σ are modified via decreased concentration of Lon protease due to CRISPRi knockdown. Bottom row indicates wild type system where Lon actively degrades MarA, producing time-series changes in protein concentration. **(E)** Experimental results showing differences in activator variability between wild type and CRISPRi systems. Dots show mean coefficient of variation over n = 5 growing microcolonies. Shaded regions show standard error (S3 Fig). **(F)** Histograms showing distributions of P_{marA} at final time point of (E). The two distributions are statistically different by the Kolmogorov-Smirnov test, $p<0.001$. **(G)** Downstream coordination expands differently in wild type and CRISPRi strains. Mutual information between YFP and RFP (P_{inaA} and P_{acrAB}) is calculated across replicates in n = 5 growing microcolonies. Mean and standard error are represented as in (E). **(H)** Maximum coordinated diversity is increased in CRISPRi system over wild type. Bivariate scatter plots show P_{inaA} and P_{acrAB} expression levels at the final time point across n = 5 microcolonies. The two distributions are statistically different by the 2D Kolmogorov-Smirnov test, $p<0.001$. Snapshots give examples of coordination in a single microcolony. Blue is P_{inaA}, red is P_{acrAB}, downstream coordination appears as magenta. Note that lack of coordination appears as red or blue cells.

https://doi.org/10.1371/journal.pcbi.1006634.g002

Fig). The half-life of MarA under these conditions should be increased above the wild type rate of 1–3 minutes but below the *lon* knockout rate of ~30 minutes. As in other studies, we were unable to quantify the exact half-life because the unusually fast degradation rate of MarA prevents observation via Western blot in the absence of overexpression (S2 Fig). We note that the *lon* knockdown may introduce more subtle changes, therefore we use this approach in tandem with computational modeling and an alternative experimental method protecting MarA from proteolytic degradation. Decreasing Lon protease is expected to affect the correlation time τ of MarA, as well as the standard deviation of its time trace (Fig 2D). The analytical modeling requires that all chemical species are abundant enough such that the propensity functions do

not change at low copy numbers [34]. Here, we found that all fluorophores were well above background levels, indicative of non-zero gene product concentrations.

We co-transformed cells with the CRISPRi construct with a plasmid containing transcriptional reporters for MarA and its downstream genes. To report MarA levels, the plasmid contains a modified *marRAB* promoter controlling cyan fluorescent protein (*cfp*). This *cfp* is modified by the addition of an *ssrA* tag in order to decrease its half-life to align it with the dynamics of the actively degraded MarA [35]. Our analytical results predict that extending the half-life of an activator should produce increased variability in growing microcolonies. By measuring the CFP levels of individual cells in the CRISPRi knockdown system and a wild type strain we found that the half-life of MarA determines how noise expands in growing microcolonies (Fig 2E). The analytical results predict that the rate of diversity generation should not be altered in growing microcolonies, but that the maximum diversity will be (as quantified by coefficient of variation). The coefficient of variation is used to measure variability in expression as the cellular fluorescence has a non-zero mean. Moreover, dividing by the mean removes the possibility that arbitrary adjustments to the gain of the microscope would impact the results. Consistent with our analytical predictions, we found that the slope of the curves was similar, but the maximum value changes. The distribution of CFP within microcolonies at the final time step of the experiments highlights the differences in maximum diversity (Fig 2F). As in the theoretical predictions, the mean and standard deviation of MarA in the CRISPRi knockdown system, which has a longer half-life, increase compared to the wild type system.

In addition to the *marA* reporter, we also measured expression of two downstream genes: *inaA*, which is a pH-inducible gene involved in stress response [36] and *acrAB*, which is a component of the *acrAB-tolC* antibiotic efflux pump [37,38]. We selected these two genes because of their disparate functionality, yet similar dose response curves [27]. We used P_{inaA} to control expression of yellow fluorescent protein (*yfp*) and P_{acrAB} to control red fluorescent protein (*rfp*). By simultaneously measuring the dynamics of all three fluorophores (P_{marA}-*cfp*, P_{inaA}-*yfp*, P_{acrAB}-*rfp*) via time-lapse microscopy, we were able to quantify variability in the *marA* input and two outputs in both the CRISPRi and wild type systems.

We used these fluorescence data to calculate the coordinated diversity in the microcolony by measuring mutual information over time. This metric captures the value of a large spectrum of correlations between two downstream genes without over-valuing high correlations between a few cells, such as would occur during the beginning growth stages of a microcolony [26]. Mirroring the analytical results, we see that there is an advantage to increasing the half-life of MarA, where coordinated phenotypic diversity is higher between the two downstream genes in the CRISPRi strain (Fig 2G).

To emphasize the differences, we compared single-cell data from the final time point of the movies. As expected, the mean concentration of both YFP and RFP increases in the CRISPRi system relative to wild type due to decreased MarA degradation (Fig 2H). Importantly, sample snapshots of the two conditions show greater correlation between the fluorophores (higher proportion of magenta cells) in the longer half-life CRISPRi system. This illustrates that in addition to increasing mean expression of the downstream genes, the correlation between downstream gene promoter activities increases with the half-life of the activator.

These results show clear advantages for longer half-life activators (equivalent to conditions without active degradation), but they do so without constraints–the variance of the activator is allowed to increase without a limit. This may not be the case in natural systems which have a target concentration range for the activator molecule. In order to investigate this, we modified our mathematical model to create a system where the standard deviation does not increase as a function of the activator half-life. We did this by requiring the noise to be inversely related to

the correlation time $\sigma = \sqrt{2/\tau}$. This represents a system where the total variability is constrained, but where the rate at which it grows is a free parameter. Three example trajectories from stochastic simulations with varying degradation rates but normalized standard deviations show different time series behaviors that produce identical steady state distributions (Fig 3A). Under this constraint, we see that the rate at which the variance of a population develops is a function of activator half-life (Fig 3B). Moreover, when the activator variance is constrained, a short half-life activator increases mutual information faster, but plateaus sooner and at lower values than a longer half-life activator (Fig 3C). Thus, faster-degrading activators are capable of generating coordinated diversity faster, but the maximum correlation that they can produce between two downstream genes is limited. Here is the first evidence of a potential trade-off as we increase activator half-life by inhibiting active degradation: maximum coordination between two downstream targets increases but the rate at which coordination is generated decreases.

In order to verify these theoretical results experimentally, we developed a system in which we could control the mean activator concentration independently of the half-life. To this end, we employed a modified version of MarA that is resistant to degradation by Lon and placed it under the control of an inducible promoter. In this design, *marA* is translationally fused to *cfp* thereby protecting the C terminus from recognition and degradation by Lon protease [24,39]. This modified MarA has an estimated half-life of ~30 minutes compared to the wild type half-life of 1–3 minutes [24] (S2 Fig). Expressing the MarA fusion from the P_{lacUV5} promoter allowed us to tune its expression level using IPTG. Thus, we were able to tune the steady state concentration of MarA and the noise that scales with it. We transformed the MarA fusion plasmid into *E. coli* Δ*marRAB* along with a two-color version of the downstream gene reporter plasmid (P_{lacUV5}-*marA-cfp* with P_{inaA}-*yfp*, P_{acrAB}-*rfp*). By monitoring the real-time MarA level

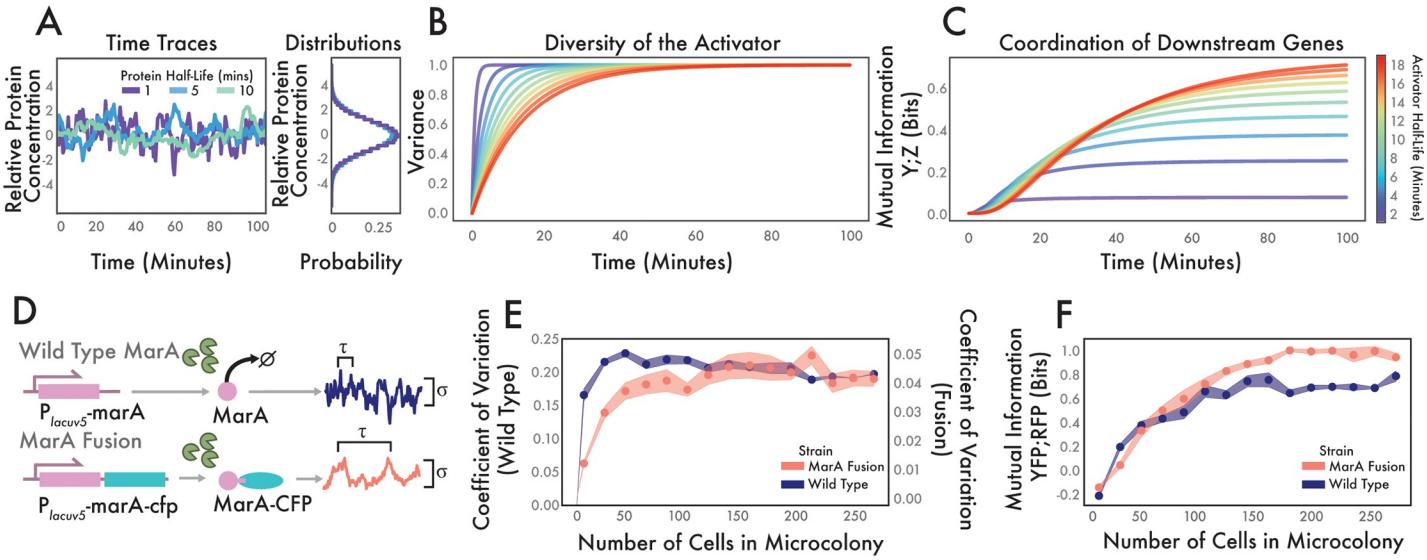


Fig 3. MarA-CFP fusion shows different downstream statistics than wild type MarA, even at similar expression levels. (A) Simulation of how modulating the half-life of regulator X affects correlation time. Sample trajectories with varying half-lives but constrained population variance produce the same distributions (right). **(B)** Analytical solutions for the variability of a protein as a function of time and half-life. **(C)** Analytical solutions for the coordination of two downstream genes as a function of differing activator half-lives. **(D)** Experimental schematic comparing wild type and MarA fusion systems. Top row indicates wild type system. Bottom row indicates protection of MarA from active degradation by Lon via a translational fusion with CFP. This modification changes the correlation time τ compared to wild type. IPTG induction of the LacUV5 promoter allows us to adjust σ independently of τ. **(E)** Experimental results showing growing variability of wild type and MarA fusion strains. **(F)** Experimental results of growing coordinated diversity of wild type and MarA fusion. For (E) and (F) dots show mean coefficient of variation over n = 5 growing microcolonies. Shaded regions show standard error. S4 Fig shows the scatter plots of the final time point for both of these strains.

https://doi.org/10.1371/journal.pcbi.1006634.g003

directly using CFP, we were able to quantify how much MarA was present in each cell. We compared this strain with altered MarA degradation to a system with wild type MarA under the control of the P_{lacUV5} promoter as well as the three-color reporter described previously (P_{lacUV5}-*marA* with P_{marA}-*cfp*, P_{inaA}-*yfp*, P_{acrAB}-*rfp*).

The two systems produce protein concentrations with different statistics over time (Fig 3D). The MarA fusion has a longer correlation time due to protection from Lon protease, however unlike in the CRISPRi system, the expression level can be tuned via IPTG induction. In experiments, we observed that wild type MarA achieved its maximum diversity faster than the MarA fusion (Fig 3E). This is in contrast to the CRISPRi knockdown system in which the rates did not change substantively as a function of half-life. This is an essential difference because the rate of activator diversity generation determines the rate of coordination in downstream targets. S2 and S3 Movies show how the growing microcolonies exhibit differences in how diversity is generated. Wild type MarA produces diversity quickly while the microcolony expressing the MarA fusion takes longer. Therefore, we see that both maximum diversity and the rate of diversity generation can be altered by modulating the half-life of the molecule.

As with the CRISPRi system, the changes in activator dynamics go on to alter how downstream genes are regulated, where increasing MarA's half-life increases the maximum coordinated diversity between downstream genes (Fig 3F). However, unlike in Fig 2G, the rate at which the wild type and MarA fusion generate coordination between downstream genes is different. We observed that the wild type strain approached its maximum degree of coordination between the two genes faster than the MarA fusion. This is a reflection of activator diversity accumulating faster when the system produces wild type MarA. Also, in contrast to the CRISPRi knockdown example, here both strains express the same steady state levels for each of the downstream genes. This shows that even if the mean expression is equivalent, the coordination between genes can be different (S4 Fig).

So far, we have compared the maximum coordinated diversity that a system can produce and the rate at which this diversity grows. The information rate is an important metric to consider because it explicitly outlines the role that a stochastic activator plays in managing the progressive development of phenotypic diversity among multiple genes. In order to conceptualize the difference between the information rate and total mutual information, consider Fig 4A showing two increasingly resolved maple leaves. We see that in the two rows, we must consider both the rate at which the image gains clarity as well as the maximum clarity of the image. Genetic networks may optimize for increased rate at the expense of low mutual information in time-sensitive conditions. Alternatively, a decreased information rate may be acceptable if time constraints are not an issue and total information is more important. To quantify this

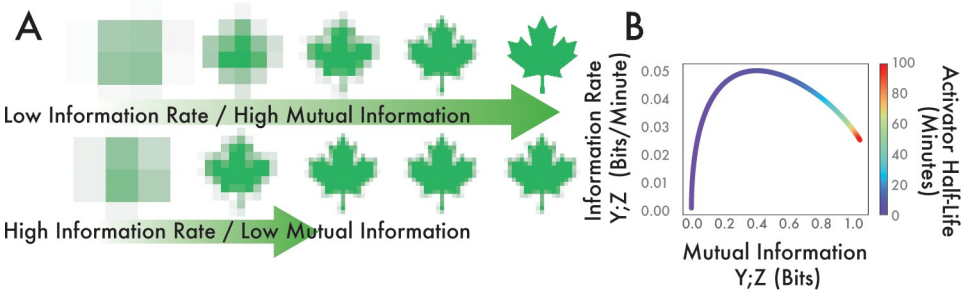


Fig 4. Trade-offs in mutual information versus information rate as a function of activator half-life. (A) Illustration of the differences between information rate and maximum information. Growing resolution of maple leaf indicates increased information. Top row has higher maximum information, but it is accrued at a lower rate as compared to the bottom row. **(B)** Mutual information and information rate between two downstream genes as a function of activator half-life.

https://doi.org/10.1371/journal.pcbi.1006634.g004

trade-off, we used the methods described in [40] to calculate the information rate for our model and compared that to the maximum information between two downstream genes. First, at extremely short half-lives both the information rate and the maximum information are very low. This is because near the uncorrelated white noise limit, the activator signal X is filtered by the downstream genes Y and Z. However, as we increase the activator half-life we see a marked increase in both information rate and mutual information. This is a function of a rapidly changing activator passing information to downstream targets, which allows them to coordinate. As the activator half-life increases further, the maximum information continues to increase monotonically while the information rate decreases. A slowly changing signal in X is passed faithfully to downstream targets but the rate of information is slow. Note however that information transmission rate is not simply the derivative of mutual information over time, as it is computed from the complete power spectra of the two signals and includes information passed with time delays [40] (Methods).

We have demonstrated how active degradation of a master regulator can change the way a growing microcolony generates coordinated phenotypic diversity. Importantly, we have highlighted a role for active degradation in increasing the rate of information transmission. However, this increased information rate comes at the cost of decreased maximum mutual information between downstream targets. Together, these opposite design demands represent a trade-off that genetic networks can optimize based on individualized requirements.

Discussion

In *E. coli*, several key regulators are subject to active degradation. We show that in the case of MarA, the half-life of a regulatory molecule affects not only its time-series behavior and population statistics, but also its ability to coordinate downstream genes. This downstream coordination develops over time, with both a rate and maximum value.

We focus on how individual founders of new bacterial populations can quickly establish a spectrum of coordinated phenotypes. We show that generating variability in downstream targets is limited by variability in the activators that control them. Also, signals from activators that change too quickly can be filtered, narrowing the spectrum of coordination in downstream targets. Our results indicate that there is a trade-off between information rate and maximum information in coordinating downstream targets. While this will depend on a number of system specific parameters, this trade-off shows that perfect information fidelity and instantaneous coordination cannot coexist. This is analogous to instructing two people to do a task in tandem–the faster you speak, the faster they can be instructed to coordinate and execute the objective, but at some point information is lost and mistakes will be made.

Although we focused on how individual genes and proteins generate phenotypic diversity, extrinsic factors like growth rate have the potential to affect this as well. For instance, varying the cell division time can affect how variability in MarA forms (S5 Fig). In effect, the analytical solutions to the variance functions represent the upper limit on how diversity develops, and decreasing the growth rate scales this curve. Moreover, the greater complexity of the combined *mar-rob-sox* regulon may affect the rate at which their shared downstream genes coordinate [23]. Expanding this study to investigate the role of each component may reveal more complex emergent effects.

While our experiments and models focused on downstream genes where the typical concentrations of MarA fall within their linear regime of activation, it should be noted that this is not true for all downstream targets of MarA. Previous research has highlighted that each downstream target possesses a unique nonlinear dose response curve as a function of MarA activation [27,32]. It may be possible for growing cells to exploit the inherent nonlinearity of each downstream gene's activation curve to better achieve the stoichiometric balance required

by downstream targets with wide ranging functions. That is to say, while multiple downstream targets may be necessary to mount an effective barrier to stressors such as antibiotic challenge, the optimal activation curves of each may be unique. This flexibility of downstream activation allows for this balance to occur despite signals coming from a single shared activator. Alternatively, it may be possible that the promoters compete for a shared pool of regulatory molecules [41]. This would produce an anti-correlation between downstream gene responses, unlike the correlated responses we observed. Still in other systems or possibly in other regimes of MarA expression, this phenomenon may be observable.

Moreover, we have focused on the role of MarA as a stochastic activator, however the concentration of MarA is also dependent on the environment [42]. Interestingly, the natural degradation rate of MarA may be below our calculated optimum for balancing between rate and information. In this case, the utility of active degradation may play a role in signal transmission as well by decreasing the response time [43,44]. For instance, active degradation may allow for a transcription factor to more accurately track a time-varying environmental signal. By erasing the memory of a previous protein level, active degradation may allow for a more responsive and agile signaling network. Alternatively, the capacity of a degraded activator to generate phenotypic diversity rapidly may be useful for a few remaining cells to regenerate diversity following antibiotic challenge.

Using a combination of single-cell time-lapse movies with multiple fluorescent reporters and analytical models we have demonstrated a role that protein half-life plays in generating single-cell variability and the ability of an activator to produce coordinated diversity in downstream genes. Our results show that both maximum coordinated diversity as well as the rate of coordination between multiple targets is dependent on activator half-life. This suggests a possible design advantage for active degradation and sheds light on how cells grow from individuals to diverse populations, while coordinating expression of related processes.

Materials and methods

Strains and plasmids

We used two strains for the experiments: wild type *E. coli* MG1655 and *E. coli* MG1655 Δ*marRAB* from [24].

In order to construct the three color reporter plasmid, we modified pNS2-σVL from [29] by placing P_{marA}, P_{inaA}, and P_{acrAB} upstream of cyan fluorescent protein (CFP), venus yellow fluorescent protein (YFP), and mCherry red fluorescent protein (RFP), respectively. All other plasmids were derived from the BioBrick library described in [45].

For the CRISPRi knockdown of Lon protease, we transformed the plasmid system from [31], using one plasmid containing the constitutively expressed *lon* targeting sgRNA and another plasmid containing dCas9 under the control of a tetracycline inducible promoter.

For the MarA fusion experiments, we cotransformed the IPTG inducible MarA-CFP translational fusion plasmid from [24] with a two-color reporter plasmid bearing P_{inaA} and P_{acrAB} controlling YFP and RFP into *E. coli* Δ*marRAB*.

Additional details on plasmid construction are available in S1 File.

Time-lapse fluorescence microscopy

Cultures were inoculated from single colonies and grown overnight at 37˚C with 200 rpm shaking in Luria-Broth (LB) medium. All strains were grown in 30 μg/ml kanamycin. In addition, strains containing the CRISPRi knockdown system were grown in the presence of 100 μg/ml carbenicillin and 30 μg/ml chloramphenicol. Strains containing the wild type or MarA fusion inducible plasmids were grown with 100 μg/ml carbenicillin in addition to 30 μg/ml kanamycin.

Overnight cultures were diluted 1:100 in selective LB medium. For the wild type or inducible MarA experiments, we added 0 μM IPTG for the MarA-CFP fusion and 10 μM IPTG for wild type MarA and grew cultures for four hours. The differences in IPTG induction allowed for similar mean concentrations with different degradation kinetics (S4 Fig). For the other experiments containing CRISPRi knockdown plasmids, cultures were refreshed for 4 hours without addition of inducer. For microscopy movies, we placed cells on 1.5% MGC low melting point agarose pads [29]. We used a Nikon Instruments Ti-E microscope to image cells at 100× magnification. Time-lapse movies were taken at a temporal resolution of every three minutes for 10 hours. We used Super Segger cell tracking software to extract fluorescence data from individual cells [46]. When computing the coefficient of variation and the mutual information of growing microcolonies of a given size, data from five replicates were combined and binned according to the number of cells in the microcolony (S3 Fig).

Stochastic simulations

We modeled the activator X and the downstream products Y and Z by:

$$\dot{x} = -\frac{x}{\tau_x} + \sigma\eta_x \tag{1}$$

$$\dot{y} = \frac{1}{\tau_y}\left(g_y x - y\right) + \sigma\eta_y \tag{2}$$

$$\dot{z} = \frac{1}{\tau_z}(g_z x - z) + \sigma\eta_z \tag{3}$$

where X represents the activator concentration and Y and Z are the concentrations of two downstream proteins. The system is assumed to start at equilibrium and models the relative changes in concentration away from that steady-state point. Moreover, the model uses continuous units of concentration, allowing the functions to be resolvable at arbitrarily small time steps [34]. X, Y, and Z mirror P_{marRAB}, P_{inaA}, and P_{acrAB} in our experimental system. τ is the correlation time of each of the downstream proteins and is proportional to the half-life (λ) of the molecule: $\tau = \lambda/\ln(2)$. g is the gain of each downstream promoter. σ is the noise scaling term, which is set equal to one in the case where the variance is not normalized by the correlation time or is allowed to inversely scale with the correlation time: $\sigma = \sqrt{\frac{2}{\tau}}$. η is a zero mean Gaussian distributed white noise random variable.

Variance

To compute the analytical solutions to the variance over time we applied the methods from [28] to Eq 1:

$$Var\{X(t)\} = \frac{\tau_x}{2}\left(1 - e^{\frac{-2t}{\tau_x}}\right) \tag{4}$$

To compute the variance for systems that converge to the same final value, we modified Eq 1 to include a normalization term:

$$\dot{x} = -\frac{x}{\tau_x} + \sqrt{\frac{2}{\tau_x}}\eta_x \tag{5}$$

Computing the variance over time from this function yields:

$$Var\{X(t)\} = 1 - e^{\frac{-2t}{\tau_x}} \tag{6}$$

Derivations for variance calculations of downstream genes can be found in S1 File.

Mutual information

Mutual information is calculated from the analytical solution to the correlation function between Y and Z:

$$Corr(y,z) = \frac{Cov(y,z)}{\sqrt{Var(\mathrm{y}) * \mathrm{Var(z)}}} \tag{7}$$

$$I(y,z) = -\frac{1}{2} ln\left(1 - Corr(y,z)^2\right) \tag{8}$$

The maximum mutual information between Y and Z is computed analytically by calculating the correlation using Eqs 2 and 3.

$$I(y,z) = -\frac{1}{2}\ln\left(1 - \left(\frac{g_y g_z\left(\frac{2\tau_z\tau_y}{(\tau_y+\tau_z)(\tau_y\tau_z-{\tau_x}^2)} - \frac{\tau_x}{((\tau_y-\tau_x)(\tau_z+\tau_x))}\right)}{2\sqrt{\left(\frac{\tau_z}{2\tau_x\tau_y} + \frac{{g_y}^2(\tau_y-\tau_x)}{2({\tau_y}^2-{\tau_x}^2))}\right)\left(\frac{\tau_z}{2\tau_x\tau_z} + \frac{{g_z}^2(\tau_z-\tau_x)}{2({\tau_z}^2-{\tau_x}^2)}\right)}}\right)^2\right) \tag{9}$$

The analytical calculations for mutual information over time in growing microcolonies can be found in S1 File.

Mutual information was calculated from experimental fluorescence data using the YFP and RFP fluorescence data and k-nearest neighbor distances (k = 3) [47].

Information rate

The information rate between downstream genes is computed using Eqs 2 and 3 and following the methods outlined in [40]. S_{yz} is the cross power spectral density between Eqs 2 and 3, S_{yy} is the power spectral density for Eq 2, and S_{zz} is the power spectral density for Eq 3:

$$R(y,z) = \frac{-1}{4\pi}\int_{-\infty}^{\infty} d\omega ln\left[1 - \frac{|s_{yz}(\omega)|^2}{s_{yy}(\omega)s_{zz}(\omega)}\right] \tag{10}$$

Computing the above power spectra and performing the integration yields the equation below, where R(y,z) is the information rate:

$$R(y,z) = \frac{1}{\tau_x}\left(\sqrt{1 + \frac{{g_y}^2\tau_x}{\tau_y}} + \sqrt{1 + \frac{{g_z}^2\tau_x}{\tau_z}} + \sqrt{1 + \frac{{g_y}^2\tau_x}{\tau_y} + \frac{{g_z}^2\tau_x}{\tau_z}} - 1\right) \tag{11}$$

Supporting information

S1 Fig. Morphology of wild type, Δ*lon*, and CRISPRi knockdown strains. Phase contrast images of microcolonies after 200 minutes of growth. Slower growth rate and increased filamentation are evident in the Δ*lon* strain.
(TIFF)

S2 Fig. Half-life quantification for MarA in CRISPRi knockdown system and MarA fusion protein. Minute markers represent when sample was taken after spectinomycin exposure.

Missing bands in the expected 32 KDa range demonstrate that MarA does not exist in sufficient quantities even at t = 0 to be assayed via Western blot in the CRISPRi knockdown system due to rapid degradation. The band at 42 KDa is associated with the MarA-CFP fusion, which is stable and appears on the Western blot. For experimental details, see S1 File.
(TIFF)

S3 Fig. Generating coefficient of variation statistics from growing microcolonies. Microcolonies were allowed to grow for 300 minutes with data taken every 3 minutes. Variance was computed for each microcolony at each time point and then plotted against the number of cells in the microcolony (orange dots). These data were then binned (gray bars) and summary statistics such as the mean coefficient of variation across microcolonies (green dots) were generated for each bin.
(TIFF)

S4 Fig. Downstream gene expression for wild type and MarA fusion strains. YFP (P_{inaA}) and RFP (P_{acrAB}) fluorescence values from growing microcolony data plotted without the time dimension. Error bars show means and standard deviations for the two bivariate distributions. 10 μM IPTG induced P_{lacUV5}-MarA elicits a very similar downstream response to 0 μM IPTG induced P_{lacUV5}-MarA-CFP translational fusion (two distributions are statistically equivalent by the 2D Kolmogorov-Smirnov test, $p>0.1$).
(TIFF)

S5 Fig. Impact of growth rate on generation of MarA variance. (A) Example simulation of a growing bacterial microcolony with a cell division time of 15 minutes. Individual trajectories show level of X. **(B)** Analytical solution to the variance functions including growth rate terms. Plot also shows the average variance for 1000 stochastic simulations with cell division. The shaded regions represent the standard error over all simulations centered around the mean for each simulation set. The solid lines represent the analytical solutions, with the gray line representing the theoretical maximum. See S1 File for growth rate functions.
(TIF)

S1 Movie. Animation of activator noise propagating to downstream targets to produce coordinated diversity. (A) Example of stochastic activator (X) expression over time. Teal line shows example trajectory; shaded gray region outlines one standard deviation around the mean. **(B)** Orange line shows example trajectory of downstream gene Y as it responds to signal from X. Orange dots show location of other example trajectories over time. Shaded gray region outlines analytical solution for standard deviation around the mean. **(C)** Purple line shows example trajectory of downstream gene Z as it responds to signal from X. Purple dots show location of other example trajectories over time. Shaded gray region outlines analytical solution for standard deviation around the mean. **(D)** Analytical solution to mutual information over time. Red dot shows current mutual information at time point in simulation. **(E)** Visualization of mutual information between downstream genes. Each gray dot shows example trajectory value between Y and Z for a given time point of the simulation. Orange and purple dots from B and C are examples of the dots here.
(MP4)

S2 Movie. Diversity in wild type MarA in a growing microcolony. (A) Example of a growing bacterial microcolony expressing CFP under control of the P_{marA} promoter. **(B)** Time traces of fluorescence for each cell in the microcolony.
(MOV)

S3 Movie. Diversity in MarA fusion in a growing microcolony. (A) Example of a growing bacterial microcolony with the MarA-CFP fusion strain. **(B)** Time traces of fluorescence for each cell in the microcolony.
(MOV)

S1 File. Supporting text, including details on plasmid design and analytical solution derivations.
(PDF)

Acknowledgments

We thank Nikit Patel and Imane El Meouche for their critical reading of the manuscript.

Author Contributions

Conceptualization: Nicholas A. Rossi, Mary J. Dunlop.

Methodology: Nicholas A. Rossi, Thierry Mora, Aleksandra M. Walczak.

Software: Nicholas A. Rossi.

Supervision: Thierry Mora, Aleksandra M. Walczak, Mary J. Dunlop.

Writing – original draft: Nicholas A. Rossi, Mary J. Dunlop.

Writing – review & editing: Nicholas A. Rossi, Thierry Mora, Aleksandra M. Walczak, Mary J. Dunlop.

References

1. Nath K, Koch AL. Protein degradation in Escherichia coli. I. Measurement of rapidly and slowly decaying components. J Biol Chem. American Society for Biochemistry and Molecular Biology; 1970 Jun 10; 245 (11):2889–900. PMID: 4912536
2. Maurizi MR. Proteases and protein degradation in Escherichia coli. Experientia. Birkhäuser-Verlag; 1992 Feb; 48(2):178–201.
3. Gottesman S. Proteases and their Targets in Escherichia coli. http://dxdoiorg/101146/annurevgenet301465. Annual Reviews 4139 El Camino Way, P.O. Box 10139, Palo Alto, CA 94303–0139, USA; 2003 Nov 28;30(1):465–506.
4. Gur E, Sauer RT. Recognition of misfolded proteins by Lon, a AAA(+) protease. Genes Dev. Cold Spring Harbor Lab; 2008 Aug 15; 22(16):2267–77. https://doi.org/10.1101/gad.1670908 PMID: 18708584
5. Bezawork-Geleta A, Brodie EJ, Dougan DA, Truscott KN. LON is the master protease that protects against protein aggregation in human mitochondria through direct degradation of misfolded proteins. Sci Rep. Nature Publishing Group; 2015; 5(1):14914.
6. Laskowska E, Kuczyńska Wiśnik D, Skórko Glonek J, Taylor A. Degradation by proteases Lon, Clp and HtrA, of Escherichia coli proteins aggregated in vivo by heat shock; HtrA protease action in vivo and in vitro. Mol Microbiol. Blackwell Science Ltd; 1996 Nov 1; 22(3):555–71. https://doi.org/10.1046/j.1365-2958.1996.1231493.x PMID: 8939438
7. Wickner S, Maurizi MR, Gottesman S. Posttranslational Quality Control: Folding, Refolding, and Degrading Proteins. Science. American Association for the Advancement of Science; 1999 Dec 3; 286 (5446):1888–93. PMID: 10583944
8. Fu GK, Smith MJ, Markovitz DM. Bacterial protease Lon is a site-specific DNA-binding protein. J Biol Chem. American Society for Biochemistry and Molecular Biology; 1997 Jan 3; 272(1):534–8. PMID: 8995294
9. Flynn JM, Neher SB, Kim Y-I, Sauer RT, Baker TA. Proteomic Discovery of Cellular Substrates of the ClpXP Protease Reveals Five Classes of ClpX-Recognition Signals. Molecular Cell. 2003 Mar; 11 (3):671–83. PMID: 12667450
10. Kafri M, Metzl-Raz E, Jona G, Barkai N. The Cost of Protein Production. Cell Reports. 2016 Jan; 14 (1):22–31. https://doi.org/10.1016/j.celrep.2015.12.015 PMID: 26725116

11. Mugler A, Kittisopikul M, Hayden L, Liu J, Wiggins CH, Süel GM, et al. Noise Expands the Response Range of the Bacillus subtilis Competence Circuit. PLoS Comput Biol. Public Library of Science; 2016 Mar; 12(3):e1004793. https://doi.org/10.1371/journal.pcbi.1004793 PMID: 27003682
12. Schrader EK, Harstad KG, Matouschek A. Targeting proteins for degradation. Nat Chem Biol. Nature Publishing Group; 2009 Nov 1; 5(11):815–22. https://doi.org/10.1038/nchembio.250 PMID: 19841631
13. Giaccia AJ, Kastan MB. The complexity of p53 modulation: emerging patterns from divergent signals. Genes Dev. Cold Spring Harbor Lab; 1998 Oct 1; 12(19):2973–83. PMID: 9765199
14. Mathes E, O'Dea EL, Hoffmann A, Ghosh G. NF-κB dictates the degradation pathway of IκBα. EMBO J. 2008 Apr 10; 27(9):1357–67. https://doi.org/10.1038/emboj.2008.73 PMID: 18401342
15. Gilmore TD. Introduction to NF-kappaB: players, pathways, perspectives. Oncogene. 2006 Oct 30; 25 (51):6680–4. https://doi.org/10.1038/sj.onc.1209954 PMID: 17072321
16. Tudelska K, Markiewicz J, czyk MKX, Czerkies M, Prus W, Korwek Z, et al. Information processing in the NF-κB pathway. Sci Rep. Springer US; 2017 Nov 15;:1–14. https://doi.org/10.1038/s41598-016-0028-x
17. Christiano R, Nagaraj N, Fröhlich F, Walther TC. Global Proteome Turnover Analyses of the Yeasts S. cerevisiae and S. pombe. Cell Reports. 2014 Dec; 9(5):1959–65. https://doi.org/10.1016/j.celrep.2014.10.065 PMID: 25466257
18. Eden E, Geva-Zatorsky N, Issaeva I, Cohen A, Dekel E, Danon T, et al. Proteome Half-Life Dynamics in Living Human Cells. Science. 2011 Feb 10; 331(6018):764–8. https://doi.org/10.1126/science.1199784 PMID: 21233346
19. Griffith KL, Shah IM, E Wolf R. Proteolytic degradation of Escherichia coli transcription activators SoxS and MarA as the mechanism for reversing the induction of the superoxide (SoxRS) and multiple antibiotic resistance (Mar) regulons. Mol Microbiol. Blackwell Science Ltd; 2004 Mar 1; 51(6):1801–16. PMID: 15009903
20. Das M, Bhaskarla C, Verma T, Kumar A, Nandi D, Mahadevan S. Roles of Lon protease and its substrate MarA during sodium salicylate-mediated growth reduction and antibiotic resistance in Escherichia coli. Microbiology. 2016 May 1; 162(5):764–76. https://doi.org/10.1099/mic.0.000271 PMID: 26944926
21. Barbosa TM, Levy SB. Differential expression of over 60 chromosomal genes in Escherichia coli by constitutive expression of MarA. J Bacteriol. American Society for Microbiology; 2000 Jun; 182(12):3467–74. PMID: 10852879
22. Martin RG, Gillette WK, Rhee S, Rosner JL. Structural requirements for marbox function in transcriptional activation of mar/sox/rob regulon promoters in Escherichia coli: sequence, orientation and spatial relationship to the core promoter. Mol Microbiol. 1999 Nov; 34(3):431–41. PMID: 10564485
23. Chubiz LM, Glekas GD, Rao CV. Transcriptional cross talk within the mar-sox-rob regulon in Escherichia coli is limited to the rob and marRAB operons. J Bacteriol. American Society for Microbiology; 2012 Sep; 194(18):4867–75. https://doi.org/10.1128/JB.00680-12 PMID: 22753060
24. Meouche El I, Siu Y, Dunlop MJ. Stochastic expression of a multiple antibiotic resistance activator confers transient resistance in single cells. Sci Rep. 2016; 6:19538. https://doi.org/10.1038/srep19538 PMID: 26758525
25. Garcia-Bernardo J, Dunlop MJ. Tunable stochastic pulsing in the Escherichia coli multiple antibiotic resistance network from interlinked positive and negative feedback loops. Miyano S, editor. PLoS Comput Biol. Public Library of Science; 2013; 9(9):e1003229–11. https://doi.org/10.1371/journal.pcbi.1003229 PMID: 24086119
26. Tkacik G, Walczak AM. Information transmission in genetic regulatory networks: a review. J Phys: Condens Matter. IOP Publishing; 2011 Apr 20; 23(15):153102–32.
27. Rossi NA, Dunlop MJ. Customized Regulation of Diverse Stress Response Genes by the Multiple Antibiotic Resistance Activator MarA. Ioshikhes I, editor. PLoS Comput Biol. Public Library of Science; 2017 Jan 6; 13(1):e1005310. https://doi.org/10.1371/journal.pcbi.1005310 PMID: 28060821
28. Gillespie DT. Exact numerical simulation of the Ornstein-Uhlenbeck process and its integral. Phys Rev E. American Physical Society; 1996 Aug 1; 54(2):2084–91.
29. Dunlop MJ, Cox RS, Levine JH, Murray RM, Elowitz MB. Regulatory activity revealed by dynamic correlations in gene expression noise. Nat Genet. 2008 Nov 23; 40(12):1493–8. https://doi.org/10.1038/ng.281 PMID: 19029898
30. Hooshangi S, Thiberge S, Weiss R. Ultrasensitivity and noise propagation in a synthetic transcriptional cascade. Proceedings of the National Academy of Sciences. National Acad Sciences; 2005 Mar 8; 102 (10):3581–6.
31. Qi LS, Larson MH, Gilbert LA, Doudna JA, Weissman JS, Arkin AP, et al. Repurposing CRISPR as an RNA-Guided Platform for Sequence-Specific Control of Gene Expression. Cell. 2013 Feb; 152 (5):1173–83. https://doi.org/10.1016/j.cell.2013.02.022 PMID: 23452860

32. Martin RG, Bartlett ES, Rosner JL, Wall ME. Activation of the Escherichia coli marA/soxS/rob Regulon in Response to Transcriptional Activator Concentration. Journal of Molecular Biology. 2008 Jul; 380 (2):278–84. https://doi.org/10.1016/j.jmb.2008.05.015 PMID: 18514222

33. Schoemaker JM, Gayda RC, Markovitz A. Regulation of cell division in Escherichia coli: SOS induction and cellular location of the sulA protein, a key to lon-associated filamentation and death. J Bacteriol. American Society for Microbiology; 1984 May; 158(2):551–61. PMID: 6327610

34. Gillespie DT. The chemical Langevin equation. The Journal of Chemical Physics. American Institute of Physics; 2000 Jun 21; 113(1):297–306.

35. Andersen JB, Sternberg C, Poulsen LK, Bjorn SP, Givskov M, Molin S. New unstable variants of green fluorescent protein for studies of transient gene expression in bacteria. Appl Environ Microbiol. 1998 Jun; 64(6):2240–6. PMID: 9603842

36. Rosner JL, Slonczewski JL. Dual regulation of inaA by the multiple antibiotic resistance (mar) and superoxide (soxRS) stress response systems of Escherichia coli. J Bacteriol. American Society for Microbiology (ASM); 1994 Oct; 176(20):6262–9. PMID: 7928997

37. Du D, Wang Z, James NR, Voss JE, Klimont E, Ohene-Agyei T, et al. Structure of the AcrAB-TolC multidrug efflux pump. Nature. Europe PMC Funders; 2014 May 22; 509(7501):512–5. https://doi.org/10.1038/nature13205 PMID: 24747401

38. Okusu H, Ma D, Nikaido H. AcrAB efflux pump plays a major role in the antibiotic resistance phenotype of Escherichia coli multiple-antibiotic-resistance (Mar) mutants. J Bacteriol. American Society for Microbiology; 1996 Jan 1; 178(1):306–8. PMID: 8550435

39. Smith CK, Baker TA, Sauer RT. Lon and Clp family proteases and chaperones share homologous substrate-recognition domains. Proceedings of the National Academy of Sciences. National Acad Sciences; 1999 Jun 8; 96(12):6678–82.

40. Tostevin F, Wolde ten PR. Mutual Information between Input and Output Trajectories of Biochemical Networks. Phys Rev Lett. American Physical Society; 2009 May 27; 102(21):218101. https://doi.org/10.1103/PhysRevLett.102.218101 PMID: 19519137

41. Stamatakis M, Adams RM, Balázsi G. A common repressor pool results in indeterminacy of extrinsic noise. Chaos: An Interdisciplinary Journal of Nonlinear Science. 2nd ed. American Institute of Physics; 2011 Dec 29; 21(4):047523.

42. Hao Z, Lou H, Zhu R, Zhu J, Zhang D, Zhao BS, et al. The multiple antibiotic resistance regulator MarR is a copper sensor in Escherichia coli. Nat Chem Biol. 2014 Jan; 10(1):21–8. https://doi.org/10.1038/nchembio.1380 PMID: 24185215

43. Alon U. Network motifs: theory and experimental approaches. Nat Rev Genet. 2007 Jun; 8(6):450–61. https://doi.org/10.1038/nrg2102 PMID: 17510665

44. Griffith KL, Shah IM, E Wolf R Jr. Proteolytic degradation of Escherichia coli transcription activators SoxS and MarA as the mechanism for reversing the induction of the superoxide (SoxRS) and multiple antibiotic resistance (Mar) regulons. Mol Microbiol. 2004 Feb 4; 51(6):1801–16. PMID: 15009903

45. Lee TS, Krupa RA, Zhang F, Hajimorad M, Holtz WJ, Prasad N, et al. BglBrick vectors and datasheets: A synthetic biology platform for gene expression. Journal of Biological Engineering 2011 5:1. BioMed Central; 2011 Sep 20; 5(1):1. https://doi.org/10.1186/1754-1611-5-1

46. Stylianidou S, Brennan C, Nissen SB, Kuwada NJ, Wiggins PA. SuperSegger: robust image segmentation, analysis and lineage tracking of bacterial cells. Mol Microbiol. 2016 Nov; 102(4):690–700. https://doi.org/10.1111/mmi.13486 PMID: 27569113

47. Kraskov A, Stögbauer H, Grassberger P. Estimating mutual information. Phys Rev E. 2004 Jun 23; 69 (6):S231–16.